Nonisothermal Crystallization Kinetics of Nucleated Poly(ethylene terephthalate)

V. D. Deshpande, Sandeep Jape

Department of Physics, University Institute of Chemical Technology, Mumbai, India

Received 28 April 2008; accepted 21 August 2008
DOI 10.1002/app.29141
Published online 22 October 2008 in Wiley InterScience (www.interscience.wiley.com).

ABSTRACT: Studies of the nonisothermal crystallization kinetics of poly(ethylene terephthalate) nucleated with anhydrous sodium acetate were carried out. The chemical nucleating effect was investigated and confirmed with Fourier transform infrared and intrinsic viscosity measurements. The Avrami, Ozawa, and Liu models were used to describe the crystallization process. The rates of crystallization, which initially increased, decreased at higher loadings of the additive. The activation energy, calculated with Kissinger's method, was lower for nucleated samples. © 2008 Wiley Periodicals, Inc. J Appl Polym Sci 111: 1318–1327, 2009

Key words: crystallization; differential scanning calorimetry (DSC); kinetics (polym.)

INTRODUCTION

The crystallization behavior is an important factor in the processing of semicrystalline thermoplastics. The speed at which crystallization takes place under particular conditions can determine the quality of the finished product. Poly(ethylene terephthalate) (PET) is a semicrystalline polymer with excellent thermal and mechanical properties, such as high chemical resistance and low gas permeability. However, because of its slow rate of crystallization, its applications in injection molding are limited. To increase the rates of crystallization, nucleating agents have to be added. These nucleating agents, typically added during processing, in addition to increasing the rates of crystallization, generally have an effect on the crystallinity, clarity, crystallite size, and hence mechanical properties of the polymer matrix. These nucleating agents generally achieve this by lowering the free energy barrier for nucleation by providing surfaces.

THEORETICAL BACKGROUND

Chemical nucleation

Several mechanisms describing nucleation in polymers have been proposed, including self-seeding,[1] surface epitaxy,[2,3] and a mechanism proposed by Binsberg[4] involving the oriented deposition of polymer chains on shallow ditches present on the surfaces of particles. However, for sodium salts, Legras and coworkers[5–7] proposed that they do not behave like typical inert heterogeneous nucleating agents but actively participate by reacting with PET and creating ionic sodium terephthalate chain ends. The authors proposed that the chain ends precipitate and act as true nucleating agents.

The following generalized reaction path was put forth by Dekoninck et al.[8] to describe the chain-scission mechanism of sodium salts:

$$2\text{PET} + \text{R—Na} \rightarrow \text{PET—COONa} + \text{PET—R} \quad (1)$$

where R can be nitric acid, aromatic carboxylic acid, or aliphatic carboxylic acid. At long mixing times

$$2\text{PET—COONa} \rightarrow \text{PET} + \text{DST} \quad (2)$$

where DST is disodium terephthalate. For sodium benzoate, Garcia[9] reported that among the reaction products, sodium terephthalate chain ends were major contributors to the nucleating effect. The nucleating effect of each component was measured in terms of its ability to increase the peak temperature of the melt crystallization exotherm. Garcia determined that the major factors governing the nucleating efficiency of an additive for PET were the alkalinity of the salt, its solubility, its ability to disperse in PET, and the thermal stability of the additive. These studies were carried out on one such nucleating agent, anhydrous sodium acetate (SA).

Crystallization kinetics

Studies of the crystallization kinetics of polymers can be performed under either isothermal or nonisothermal conditions. As most industrial processes

Correspondence to: V. D. Deshpande (vindesh2@rediffmail.com).

such as fiber spinning, extrusion, and injection molding occur under nonisothermal conditions, studies of nonisothermal crystallization kinetics are of practical relevance.

In nonisothermal crystallization, with differential scanning calorimetry (DSC), the relative crystallinity as a function of temperature [$X(T)$] is defined as follows:

$$X(T) = \int_{T_0}^{T} (dH/dT)dT \Big/ \int_{T_0}^{T_\infty} (dH/dT)dT \qquad (3)$$

where dH is the enthalpy of crystallization released in infinitesimal temperature range dT and T_0 and T_∞ are the temperatures at which crystallization starts and ends, respectively.

If we assume that the sample experiences the same thermal history designated by the DSC furnace, the relation between crystallization time t and sample temperature T can be formulated as follows:

$$t = (T_0 - T)/\phi \qquad (4)$$

where T_0 is an arbitrary reference melting temperature and ϕ is the cooling rate. According to eq. (4), the horizontal temperature axis in a DSC thermogram for nonisothermal crystallization data can be transformed into a timescale.

The Avrami equation was initially proposed to describe nucleation and growth in metals but has been adapted to describe the crystallization process in polymers. The Avrami equation,[10–12] which is primarily used to describe the isothermal crystallization process, has the following form:

$$1 - X(t) = \exp(-kt^n) \qquad (5)$$

where $X(t)$ is the relative crystallinity as a function of time, parameter k is the Avrami rate constant, and Avrami exponent n denotes a mechanism constant that depends on the type of nucleation (homogeneous or heterogeneous) and the growth dimension (rod, disk, sphere, sheaf, etc.)

Taking logarithms, we can transform eq. (5) into the following form:

$$\log\{-\ln[1 - X(t)]\} = n \log t + \log k \qquad (6)$$

Plotting the first term $\log\{-\ln[1 - X(t)]\}$ as a function of $\log t$, we can obtain the kinetic parameters n and k.

Although the Avrami equation is often used to describe the isothermal crystallization behavior of a semicrystalline polymer, it has also been applied to describe the nonisothermal crystallization behavior of semicrystalline polymers.[13–15]

As the nonisothermal crystallization depends on the cooling rate, the crystallization rate constant (k) can be properly corrected to obtain the corresponding rate constant at a unit cooling rate (Z_c) based on the relation put forth by Jeziorny:[16]

$$\log Z_c = \log k/\Phi \qquad (7)$$

where Φ is the cooling rate. Ozawa[17] extended the Avrami theory to be able to describe the nonisothermal crystallization for a sample cooled at a constant rate from the molten state:

$$1 - X(T) = \exp[-K(T)/\Phi^m] \qquad (8)$$

where $K(T)$ and m are the Ozawa crystallization rate constant and the Ozawa exponent, respectively. The Ozawa kinetic parameters (i.e., K and m) have physical meanings similar to those of the Avrami parameters. The Ozawa kinetic parameters can be extracted from a plot of $\ln\{-\ln[1 - X(T)]\}$ versus $\ln 1/\Phi$ at a fixed temperature; K and m can be determined from the y intercept and the slope, respectively.

Furthermore, Liu et al.[18] proposed a different kinetic model by combining the Ozawa and Avrami equations; the following equation was obtained:

$$\ln K(T) - m \ln \phi = \ln k + n \ln t \qquad (9)$$

$$\ln \phi = \ln F(T) - a \ln t \qquad (10)$$

where $F(T) = [K(T)/k]^{1/m}$ refers to the value of the cooling rate chosen at a unit crystallization time at which the system has a certain degree of crystallinity and a is the ratio of n to m (i.e., n/m). According to eq. (10), at a given degree of crystallinity, a plot of $\ln \phi$ versus $\ln t$ will give a straight line with an intercept of $\ln F(T)$ and a slope of a.

Activation energy for nonisothermal crystallization

In nonisothermal crystallization processes, the Kissinger's method,[19] which considers the variation of the peak temperature of the crystallization exotherm (T_p) with the cooling rate, has been widely applied in evaluating the overall effective energy barrier (ΔE):

$$\frac{d[\ln\left(\Phi/T_p^2\right)]}{d\left(1/T_p\right)} = -\frac{\Delta E}{R} \qquad (11)$$

where R is the universal gas constant (8.314 J mol^{-1} K^{-1}). The slope of the plot of $\ln \Phi/{T_p}^2$ versus $1/T_p$ yields ΔE.

EXPERIMENTAL

Sample preparation

PET was a gift from the PET division of Reliance Industries, Ltd. (Patalganga, India). SA was obtained from S.D. Fine Chemicals, Ltd. (Mumbai, India). The polymer and the salt were dried at 110°C for 4 h

before blending. The blending was carried out in a Haake Minilab (Thermo Electron Corporation, Karlsruhe, Germany) at 280°C and 80 rpm. The polymer was mixed for 5 min before the salt was added. The samples were extruded and quenched in cold water for 5 min after the addition of the salt.

DSC studies

The crystallization studies were carried out with a PerkinElmer (Waltham, MA) DSC-7 instrument operating under a continuous nitrogen flow of 0.5 kg/cm^2. Throughout the experiment, the sample weight was kept constant at 7 mg. The instrument was calibrated for each scanning rate with an indium standard. The crystallization studies were carried out for pure PET and PET nucleated with 0.5, 1, 3, 5, or 10 wt % SA.

The nonisothermal program involved scanning each sample at different rates: 2, 5, 10, 20, 30, 40, 50, and 60°C/min. The samples were heated at a specific rate from 50 to 300°C, at which they were held for 5 min to ensure complete melting, and then they were cooled back to 50°C at the same rate as the heating rate.

Fourier transform infrared (FTIR) studies

The samples that were extruded from the miniblender were used for the preparation of films. The film-making procedure involved placing a sample in a specially fabricated oven with access from the top. The sample was first allowed to melt, and then a piece of a Teflon sheet was placed on top of it. The Teflon, upon which a coating of the PET melt had formed, was then quenched in cold water. The entire process took about 1 min to complete. The films obtained with this procedure were used for IR analysis with a PerkinElmer Spectrum 100. The FTIR spectra of pure PET and SA, as well as the nucleated samples before and after electronic subtraction, are displayed in Figures 1 and 2. The spectrum of SA was obtained after dispersion in KBr. The electronic subtraction was carried out by subtraction of the spectrum of pure PET from that of nucleated PET with the 1950-cm^{-1} band as the reference peak.[8]

IR analysis

The FTIR spectra in Figure 2 show the presence of a peak at 1593 cm^{-1} as well as a broad peak at 1548 cm^{-1}. The peaks were attributed to aromatic C=C stretching and carboxylate asymmetric stretching, respectively, by Dekoninck et al.[8] The authors related the presence of the 1593-cm^{-1} peak to the formation of sodium terephthalate chain ends. They also proposed that the higher the absorbance is, the higher the nucleating efficiency is. The nucleating

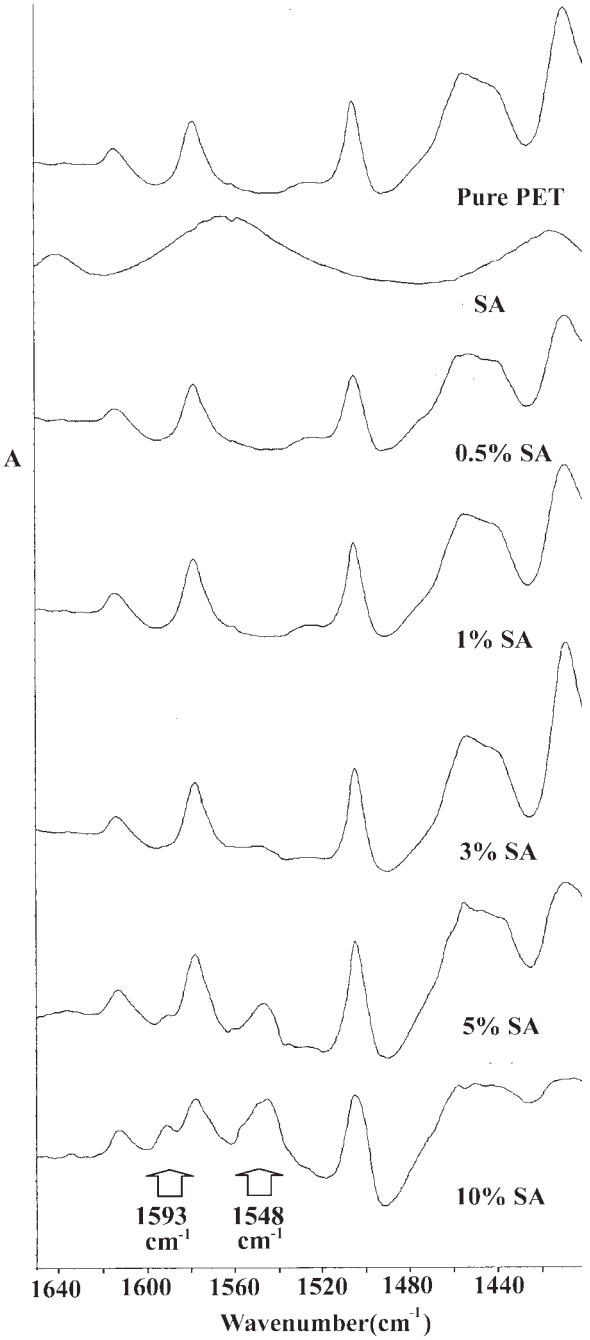

Figure 1 FTIR absorption spectra of the samples (arbitrary units).

efficiency was measured in terms of the additive's ability to reduce the cold crystallization temperature and increase the melt crystallization temperature. Figures 1 and 2 reveal a similar increase in the 1593-cm^{-1} absorbance with an increasing concentration of the nucleating agent. Initially, up to 1% SA, the 1548-cm^{-1} peak and the 1593-cm^{-1} peak were of equivalent intensity. However, beyond 3% SA, the 1548-cm^{-1} peak showed a faster increase in intensity versus the 1593-cm^{-1} peak. This could be attributed to the broadening of the 1557-cm^{-1} peak of the

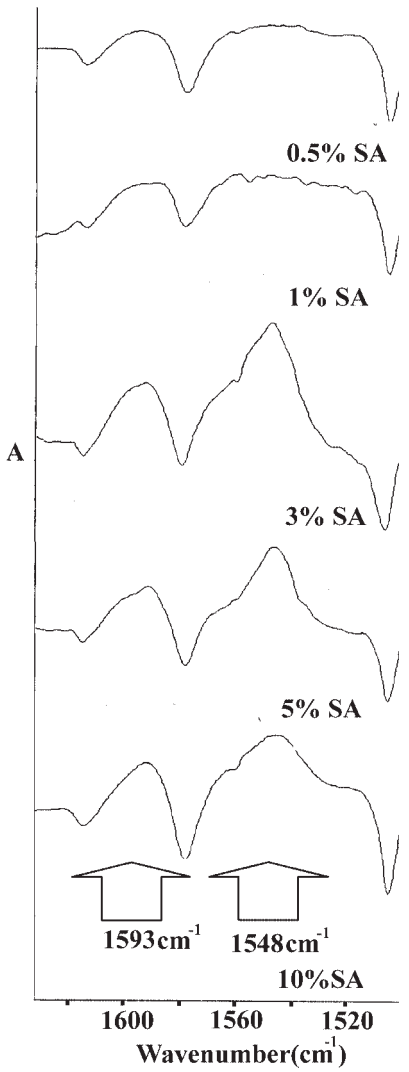

Figure 2 FTIR absorption spectra of the samples after electronic subtraction (arbitrary units).

unreacted SA, the concentration of which would keep increasing for the higher weight fraction of the additive because of incomplete dissolution.

Intrinsic viscosity

The intrinsic viscosity measurements were carried out with an Ubbelohde tube. The flow time was recorded for dilute solutions of PET in 60/40 phenol/1,1,2,2 tetrachloroethane at 30°C. The intrinsic viscosity was determined from a single concentration with the following Billmeyer relation:[20]

$$\text{Intrinsic viscosity} = \frac{0.25(\eta_{rel} - 1 + 3\ln\eta_{rel})}{c} \quad (12)$$

where $\eta_{rel} = t/t_0$ is the relative viscosity, t is the flow time of the polymer, t_0 is the flow time of the solvent, and c is the concentration (g/dL).

TABLE I
Intrinsic Viscosities of the Samples

Sample	Intrinsic viscosity (dL/g)
Pure PET	0.61
0.5% SA	0.56
1% SA	0.48
3% SA	0.41
5% SA	0.33
10% SA	0.23

The sample concentration was kept at 0.5 g/dL. The results of the intrinsic viscosity measurements are given in Table I. The intrinsic viscosity decreased as the concentration of the nucleating agent was increased. This could be attributed to the reduction in the molecular weight as a result of the reaction between PET and SA. This reaction resulted in the chain scission of PET and the formation of sodium terephthalate chain ends, the presence of which was confirmed by the FTIR results.

DSC analysis

The quenching procedure resulted in amorphous samples. Hence, when the samples were subsequently heated during the DSC run, they exhibited a cold crystallization exotherm. The variation of the peak of the cold crystallization exotherm (T_{ch}) with SA (wt %) is described in Figure 3. The peak shifted toward the lower temperature side as the concentration of nucleating agents was increased, and this typically indicates an increased crystallization rate. The values of T_p, that is, the peak of the crystallization exotherm, are presented in Figure 4. An increase in the nucleating agent caused an increase in T_p. However, for higher concentrations (3–10%), an increase in the loading led to only a moderate increase in T_p. The variations of the initial slope of

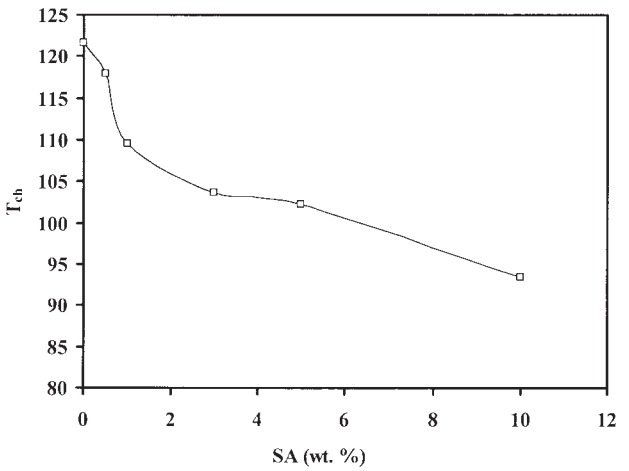

Figure 3 Effect of the SA concentration (wt %) on T_{ch} at a 2°C/min cooling rate.

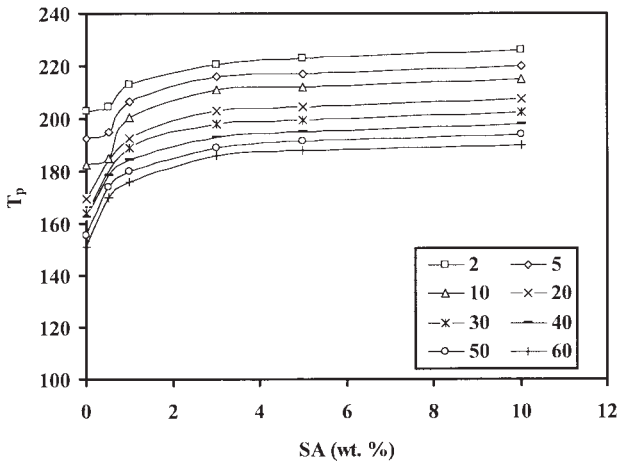

Figure 4 Effect of the SA concentration (wt %) on T_p at different cooling rates (°C/min).

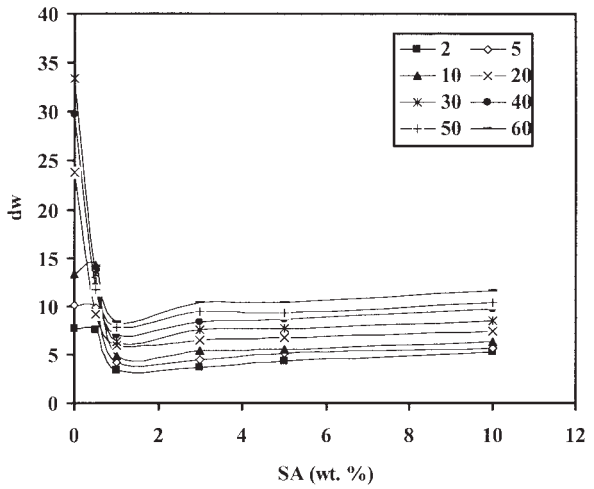

Figure 6 d_w versus SA (wt %) at different cooling rates (°C/min).

the crystallization exotherm (S_i) as well as the peak width at half-height (d_w) are described in Figures 5 and 6. S_i depends on the rate of the nucleation process, whereas d_w is the measure of the crystallite size distribution.[21–26] S_i initially showed a continuous increase up to 1% SA and subsequently decreased with an increasing concentration of the nucleating agent. d_w, although decreasing initially until 1% SA, increased with increasing concentration. This could be attributed to the fact that the increase in the nucleation rate represented by S_i provided less time for the crystallites to grow in size and hence led to a narrower (more homogeneous) distribution of the crystallites; whereas beyond 1% SA, the decrease in S_i gave rise to the creation of nuclei at different times, which ultimately grew into crystallites of widely differing sizes.[26]

The curves were converted into a timescale. Figures 7 and 8 display the broadness of the transition (Δb) and the normalized value of the enthalpy of crystallization (ΔH_c). Δb corresponds to the difference between the onset time (t_{onset}) and end time (t_{end}), that is, $\Delta b = t_{end} - t_{onset}$. Normalized ΔH_c refers to the enthalpy of crystallization that is normalized to the weight fraction of PET in the sample. Although Δb can be considered the measure of the overall rate of crystallization, normalized ΔH_c can be considered a measure of the degree of crystallinity.[22] For a particular cooling rate, the normalized ΔH_c values increased with the addition of the nucleating agent. This implied an increased level of crystallinity. Δb decreased with increasing concentration, reaching a minimum at 1% SA, beyond which it increased. This indicated that the highest overall crystallization rates were achieved for 1% SA.

Avrami analysis

Figure 9 shows plots of the relative crystallinity with time for PET with different concentrations of SA.

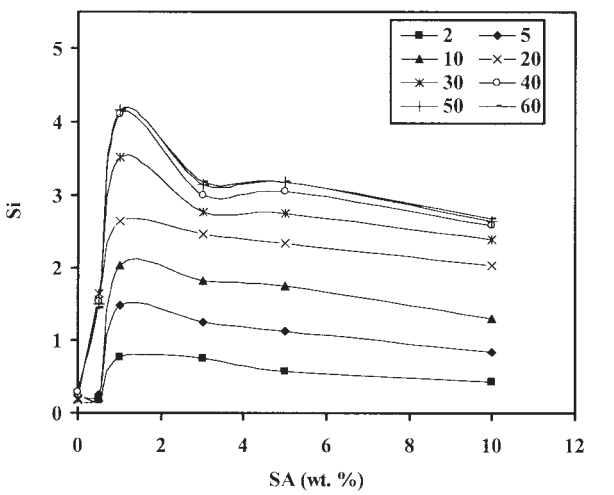

Figure 5 S_i versus SA (wt %) at different cooling rates (°C/min).

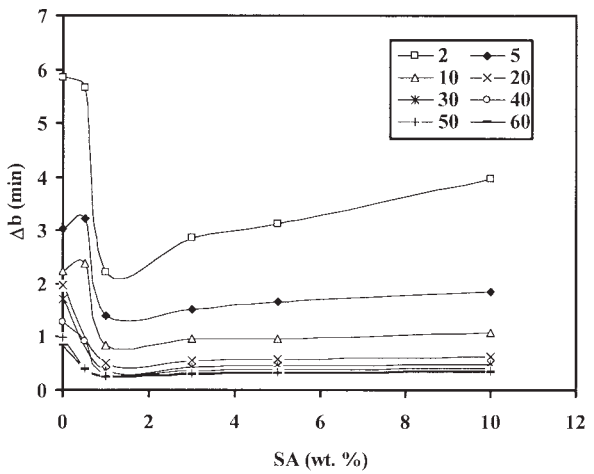

Figure 7 Δb versus SA (wt %) at different cooling rates (°C/min).

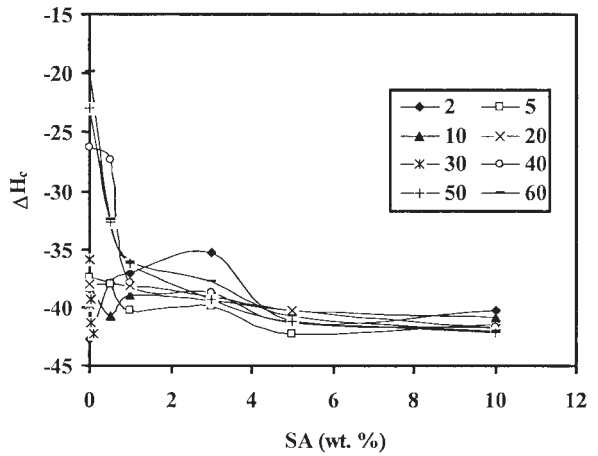

Figure 8 Normalized values of ΔH_c (J/g) versus SA (wt %) at different cooling rates (°C/min).

After an initial delay, the curves show a linear nature that corresponds to the primary crystallization stage. The observed nonlinear behavior at the end can be attributed to secondary crystallization. The curves corresponding to PET nucleated with SA shift toward the shorter timescale. However, for higher concentrations of SA, the crystallization process seemed to take an increasingly longer time to complete. Also, the plots show that as the concentration of the nucleating agent was increased beyond 1% SA, the secondary crystallization had a greater role in the crystallization process. The decrease in the nucleation rates, resulting in the formation of crystallites of widely differing sizes, led to the increasingly longer secondary crystallization stage. At lower concentrations of the additive, particularly at 1% SA, an increase in the nucleation rate and a narrower, more homogeneous distribution of crystallites resulted in the secondary crystallization stage being not as prominent.

A typical Avrami plot is shown in Figure 10. The plots show a linear nature; the observed nonlinear behavior can be attributed to secondary crystallization. Because the Avrami equation describes the primary crystallization until impingement, only the straight portion of the graph corresponding to 30–70% conversion was considered for analysis. n and k were obtained from the slope and intercept, respectively. The values of k, n, $t_{0.5}$ (half-time of crystallization), and Z_c are listed in Table II. For a particular cooling rate, the values of k increased with the addition of the nucleating agent up to 1% SA. However, the rates also showed a decrease with increasing concentrations higher than 1% SA. For a particular cooling rate, the values of $t_{0.5}$ (the time taken for 50% conversion) reached a minimum at 1% SA and then increased with increasing concentration, once again indicating that the highest rates were achieved for PET nucleated with 1% SA. The rate constant per unit of the cooling rate followed a similar pattern. However, its values remained close to 1 for cooling rates higher than 30°C/min.

From Table II, it can be seen that in the nucleated samples, n for a particular cooling rate, which initially tended to increase, decreased for higher concentrations. The exponent values ranged from 3 to 4, remaining close to 3 for higher concentrations; this corresponded to three-dimensional growth with heterogeneous nucleation. n was affected by the nature of the nucleation (heterogeneous and homogeneous) as well as the geometry of the crystals. High exponent values at lower concentrations would suggest more sporadic nucleation. However, studies of the morphology would be required for an adequate explanation.

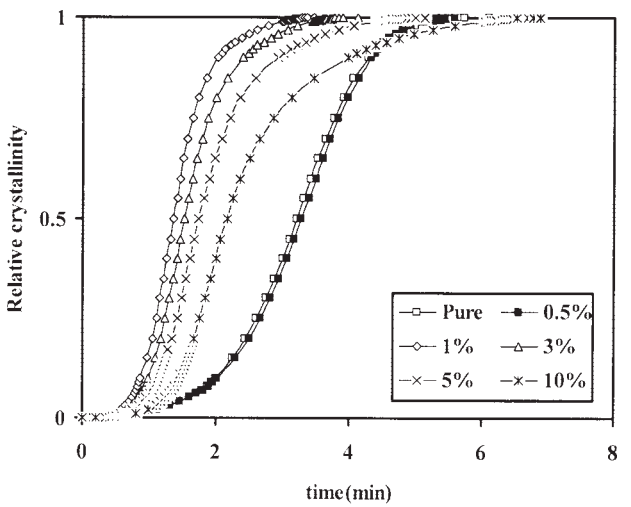

Figure 9 Relative crystallinity versus time for PET with different concentrations of SA at a 5°C/min cooling rate.

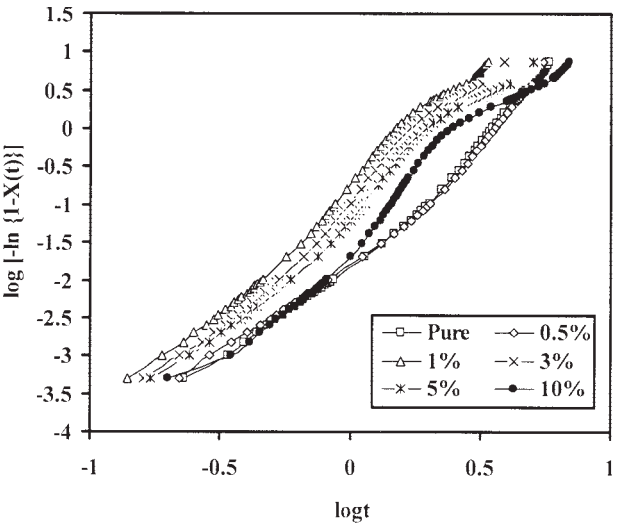

Figure 10 Avrami plots for PET with different concentrations of SA at a 5°C/min cooling rate.

TABLE II
Parameters of Nonisothermal Crystallization Kinetics with the Avrami and Jeziorny Models

Sample	Cooling rate (°C/min)	k (min^{-n})	n	r^2	$t_{0.5}$ (min)	Z_c
Pure PET	2	2.69×10^{-5}	4.98	0.9999	7.7	5.18×10^{-3}
	5	4.43×10^{-3}	4.33	0.9997	3.21	3.38×10^{-1}
	10	4.55×10^{-2}	3.91	0.9998	2.01	7.34×10^{-1}
	20	2.58×10^{-1}	3.20	0.9997	1.36	9.34×10^{-1}
	30	6.22×10^{-1}	2.62	0.9998	1.04	9.84×10^{-1}
	40	1.37	2.60	0.9951	0.76	1.01
	50	2.24	2.86	0.998	0.66	1.02
	60	3.01	3.06	0.9998	0.62	1.02
			3.44 (average)			
0.5% SA	2	8.79×10^{-3}	3.01	1	4.26	9.37×10^{-2}
	5	3.67×10^{-5}	4.41	0.9998	3.28	1.30×10^{-1}
	10	3.67×10^{-2}	3.90	0.9997	2.13	7.18×10^{-1}
	40	4.63	2.06	0.9807	0.39	1.04
	50	8.13	2.45	0.9827	0.36	1.04
	60	8.84	2.28	0.9884	0.32	1.04
			3.02 (average)			
1% SA	2	9.07×10^{-3}	4.20	0.9998	2.8	9.52×10^{-2}
	5	1.93×10^{-1}	4.04	0.9993	1.37	7.19×10^{-1}
	10	9.10×10^{-1}	4.59	0.9984	0.94	9.91×10^{-1}
	20	8.35	4.26	0.9921	0.55	1.11
	30	3.70×10^{1}	4.48	0.9907	0.41	1.13
	40	9.30×10^{1}	4.44	0.9966	0.33	1.12
	50	2.04×10^{2}	4.17	0.971	0.25	1.11
	60	1.88×10^{2}	3.73	0.9792	0.22	1.09
			4.24 (average)			
3% SA	2	2.91×10^{-2}	3.44	0.998	2.5	1.71×10^{-1}
	5	1.30×10^{-1}	3.86	0.9958	1.53	6.65×10^{-1}
	10	8.81×10^{-1}	3.94	0.9957	0.93	9.87×10^{-1}
	20	5.74	3.94	0.9944	0.58	1.09
	30	1.87×10^{1}	4.25	0.9907	0.46	1.10
	40	3.78×10^{1}	4.26	0.9909	0.39	1.10
	50	5.85×10^{1}	4.29	0.987	0.35	1.08
	60	6.31×10^{1}	3.49	0.9914	0.27	1.07
			3.94 (average)			
5% SA	2	5.66×10^{-3}	3.71	0.9948	3.63	7.52×10^{-2}
	5	9.01×10^{-2}	3.59	0.9931	1.75	6.18×10^{-1}
	10	9.48×10^{-2}	3.83	0.994	0.96	7.90×10^{-1}
	20	6.21	3.74	0.9947	0.55	1.10
	30	1.48×10^{1}	4.15	0.9951	0.48	1.09
	40	3.01×10^{1}	3.78	0.9939	0.37	1.09
	50	5.59×10^{1}	4.37	0.985	0.36	1.08
	60	5.45×10^{1}	3.69	0.9911	0.31	1.07
			3.86 (average)			
10% SA	2	5.13×10^{-3}	3.27	0.9856	4.43	7.16×10^{-2}
	5	5.06×10^{-2}	3.32	0.9858	2.17	5.51×10^{-1}
	10	5.45×10^{1}	3.51	0.9896	1.1	1.49
	20	2.86	3.59	0.9888	0.67	1.05
	30	8.63	3.55	0.9982	0.49	1.07
	40	1.68×10^{1}	3.45	0.9931	0.39	1.07
	50	2.76×10^{1}	3.45	0.9848	0.34	1.07
	60	3.67×10^{1}	3.28	0.9799	0.29	1.06
			3.58 (average)			

Ozawa analysis

From the values of $X(T)$ calculated with eq. (3), Ozawa plots were obtained. A representative Ozawa plot of pure PET and a 1% SA sample is shown in Figure 11(a,b). There is a significant deviation from the linear nature with the addition of the nucleating agent. The points at the bottom of the curve correspond to the beginning of the crystallization process at higher cooling rates, whereas the points at the top correspond to nearly the end of the crystallization process for low cooling rates; this causes curvature of the plots. Another factor affecting the plots is the secondary crystallization in the nucleated samples,

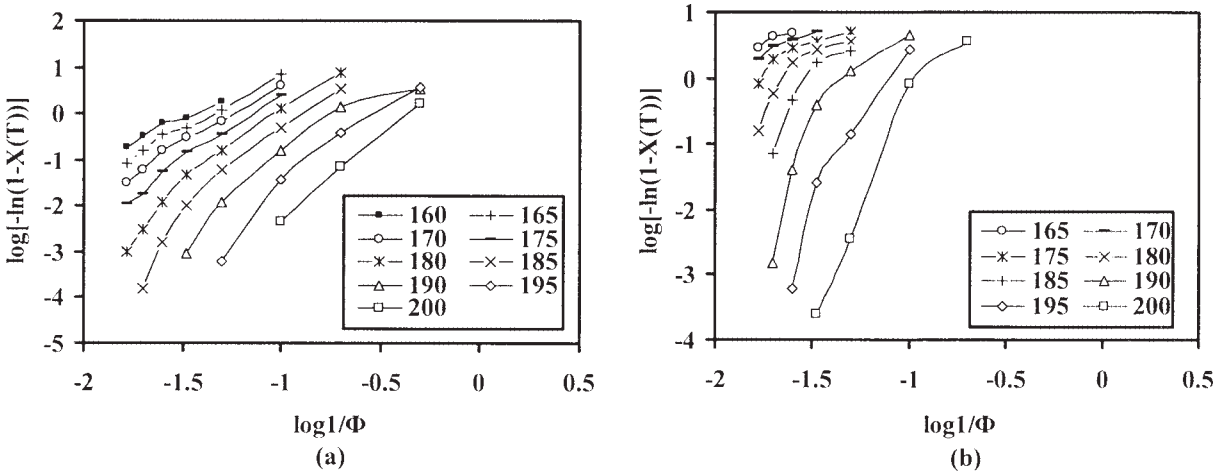

Figure 11 Ozawa plots for (a) pure PET and (b) PET plus 1% SA.

which is neglected in the Ozawa approach. Hence, it does not describe the crystallization process in the nucleated samples satisfactorily.

Liu's analysis

Figure 12 shows Liu's plots of ln ϕ versus ln t. A linear fit suggests that Liu's procedure might be useful in modeling the nonisothermal crystallization kinetics. From the slope and intercept of the plot, we obtained the values of a and $F(T)$, which are listed in Table III. $F(T)$ refers to the value of the cooling rate chosen at a unit crystallization time when the system has a certain degree of crystallinity.

The $F(T)$ values underwent a minimum at 1% SA and subsequently increased with increasing concentration, indicating that the highest rates were achieved at this concentration. The values of $F(T)$ also systematically increased with an increasing relative degree of crystallinity, and this indicates that, at the unit crystallization time, a higher cooling rate should be used to obtain a higher degree of crystallinity. The linear nature of the plots is reflected in the good correlation coefficient values. The values of a, which is the ratio of n to m, do not show significant variation. Thus, Liu's analysis seems fairly successful in describing the crystallization process. However, it does not give any information regarding the geometry of the crystallites.

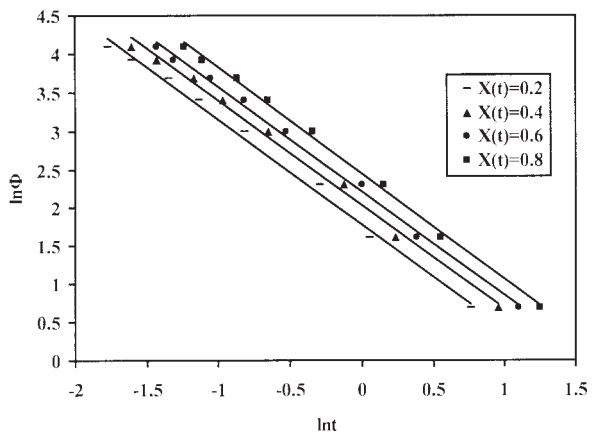

Figure 12 Liu plots for 1% SA.

Kissinger analysis

The values of the activation energy for crystallization are listed in Table IV. The activation energy, which had negative values, decreased with the concentration increasing, leveling off at 3% SA. For

TABLE III
Parameters of Nonisothermal Crystallization Kinetics from the Liu Analysis

Sample	$X(t)$	a	$F(T)$	r^2
Pure PET	0.2	1.29	18.24	0.9936
	0.4	1.34	25.39	0.9937
	0.6	1.39	32.39	0.9937
	0.8	1.46	44.53	0.9887
0.5% SA	0.2	1.10	10.86	0.9465
	0.4	1.11	14.29	0.9542
	0.6	1.16	18.05	0.964
	0.8	1.08	19.90	0.9548
1% SA	0.2	1.36	5.97	0.9939
	0.4	1.11	7.62	0.9949
	0.6	1.16	9.18	0.9964
	0.8	1.08	11.54	0.9972
3% SA	0.2	1.59	5.88	0.9937
	0.4	1.56	7.94	0.9953
	0.6	1.56	10.09	0.9971
	0.8	1.08	13.54	0.9976
5% SA	0.2	1.38	7.48	0.9877
	0.4	1.37	9.63	0.9903
	0.6	1.37	11.91	0.9911
	0.8	1.35	15.61	0.9935
10% SA	0.2	1.24	9.02	0.9985
	0.4	1.24	11.28	0.9985
	0.6	1.24	13.91	0.998
	0.8	1.22	18.55	0.9972

TABLE IV
Activation Energy Calculated with Kissinger's Analysis

Sample	Activation energy (kJ/mol)	r^2
Pure PET	−117.24	0.9856
0.5% SA	−158.63	0.9906
1% SA	−171.88	0.9687
3% SA	−181.84	0.9565
5% SA	−186.30	0.9659
10% SA	−184.59	0.9586

crystallization during cooling, many authors have ignored the negative sign, reporting the absolute values instead.[27,28] However, some have reported negative values of the activation energy.[29,30] Vyazovkin[31] suggested that the procedure for dropping the negative sign corresponding to negative heating rates in the Kissinger analysis is invalid. In another study involving determining the activation energy of PET with an isoconversional method,[32] the author reported that the activation energy exhibited anti-Arrhenius behavior (negative values). In this context, we decided to keep the negative sign, particularly as it complements the trend followed by the overall crystallization rate (k). A decrease in the effective energy barrier would suggest that the crystallization process should get easier.

RESULTS AND DISCUSSION

Crystallization from the melt comprises two main mechanisms: primary nucleation and crystal growth, which is controlled secondary nucleation. The nucleation rate depends on ΔG, which is the free energy barrier for the formation of the critical nucleus, as well as ΔF, which is the energy barrier affecting the transport of materials across the crystal–liquid interface through the following relation:[33]

$$I = I_0 \exp(-\Delta F/kT) \exp(-\Delta G/kT) \qquad (13)$$

where I_0 is a parameter that is temperature-independent. Generally, nucleation on a foreign surface lowers ΔG by lowering the surface free energy of the nucleus. In this study, DSC analysis revealed that the values of T_p, which increased almost linearly for lower concentrations (up to 1% SA), showed moderate increases for higher concentrations (3–10% SA). Also, the bulk crystallization rates, represented by k, decreased for concentrations beyond 1% SA. This trend may be explained as follows: an increase in the precipitated sodium terephthalate chain ends raised the value of T_p by promoting the formation of a greater number of nuclei at higher temperatures because of the strong reduction in ΔG. At lower concentrations, higher solubility and better dispersion, combined with increased chain mobility as a result of a decrease in the molecular weight, led to high nucleation and crystallization rates, the highest rates being observed at 1% SA.

At higher concentrations of SA, an increase in the concentrations of the chain ends was accompanied by an increase in unreacted SA because of incomplete dissolution. The SA particles, by tending to agglomerate, may have hindered the mobility of the polymer chains, and this affected the transport of the segments (ΔF) to the site of crystallization. This led to diminishing nucleating efficiency and resulted in a moderate increase in the values of T_p from concentrations of 3–10% SA as well as a decrease in the nucleation rates represented by the values of S_i, which decreased for concentrations beyond 1% SA.

Hence, the bulk crystallization rate represented by k, which depends on both the nucleation and spherulite growth rates, is retarded at higher concentrations of the nucleating agent. The increasing contribution of the slower secondary crystallization stage in the crystallization process also contributes to the decrease in the overall crystallization rates. However, this effect is not reflected in the values of k of the Avrami equation, which describes primary crystallization.

The Kissinger analysis revealed the effective energy barrier for crystallization, decreased with the addition of SA. The overall crystallization activation energy is the sum of the activation energies of the nucleation and crystal growth processes. At lower concentrations of SA, the precipitated sodium terephthalate chain ends, by promoting heterogeneous nucleation through the lowering of the free energy barrier of critical nuclei, caused a decrease in the overall activation energy. At higher concentrations of SA, with the agglomerates of the unreacted SA affecting the diffusion of the polymer chains, it led to the leveling of the values of the overall activation energy.

CONCLUSIONS

The chemical nucleating effect of SA was confirmed. The nucleating agent was effective in increasing the crystallization rates up to 1% SA. However, at higher loadings, the rates decreased. The highest crystallization rates were achieved for PET nucleated with 1% SA. The Avrami and Liu models well described the crystallization process, with the Liu model showing a better correlation factor.

References

1. Vidotto, G.; Levy, D.; Kovacs, A. J. Kolloid Z Z Polym 1969, 230, 289.
2. Wittmann, J. C.; Lotz, B. J Polym Sci Polym Phys Ed 1981, 19, 1837.
3. Wittmann, J. C.; Lotz, B. J Polym Sci Polym Phys Ed 1981, 19, 1853.

4. Binsbergen, F. L. J Polym Sci Polym Symp 1977, 59, 11.
5. Legras, R.; Mercier, J. P.; Nield, E. Nature 1983, 304, 432.
6. Legras, R.; Bailly, C.; Daumerie, M.; Dekoninck, J. M.; Mercier, J. P.; Zichy, V.; Nield, E. Polymer 1984, 25, 835.
7. Legras, R.; Dekoninck, J. M.; Vanzieleghem, A.; Mercier, J. P.; Nield, E. Polymer 1986, 27, 109.
8. Dekoninck, J. M.; Legras, R.; Mercier, J. P. Polymer 1989, 30, 910.
9. Garcia, D. J Polym Sci Polym Phys Ed 1984, 22, 2063.
10. Avrami, M. J Chem Phys 1939, 7, 1103.
11. Avrami, M. J Chem Phys 1940, 8, 212.
12. Avrami, M. J Chem Phys 1941, 9, 177.
13. Supaphol, P. J Appl Polym Sci 2000, 78, 338.
14. Supaphol, P.; Dangseeyun, N.; Srimoaon, P.; Nithitanakul, M. Thermochim Acta 2003, 406, 207.
15. Apiwanthanakorn, N.; Supaphol, P.; Nithitanakul, M. Polym Test 2004, 23, 817.
16. Jeziorny, A. Polymer 1978, 19, 1142.
17. Ozawa, T. Polymer 1971, 12, 150.
18. Liu, T.; Mo, Z.; Wang, S.; Zhang, H. Polym Eng Sci 1997, 37, 568.
19. Kissinger, H. E. J Res Natl Bur Stand 1956, 57, 217.
20. Billmeyer, F. W. J Polym Sci 1949, 4, 83.
21. Beck, H. N.; Ledbetter, H. D. J Appl Polym Sci 1965, 9, 2131.
22. Gupta, A. K.; Gupta, V. B.; Peters, R. H.; Harland, W. G.; Berry, J. P. J Appl Polym Sci 1982, 27, 4669.
23. Gupta, A. K.; Purwar, S. N. J Appl Polym Sci 1984, 29, 1595.
24. Gupta, A. K.; Ratnam, B. K. J Appl Polym Sci 1991, 42, 297.
25. Choudhary, V.; Varma, H. S.; Varma, I. K. J Therm Anal 1987, 32, 572.
26. Gupta, A. K.; Rana, S. K.; Deopura, B. L. J Appl Polym Sci 1992, 44, 719.
27. Balamurugan, G. P.; Maiti, S. N. J Appl Polym Sci 2008, 107, 2414.
28. Liu, Y.; Yang, Q.; Li, G. J Appl Polym Sci 2008, 109, 782.
29. Ke, Y.-C.; Wu, T.-B.; Xia, Y.-F. Polymer 2007, 48, 3324.
30. Achilias, D. S.; Papageorgiou, G. Z.; Karayannidis, G. P. J Polym Sci Part B: Polym Phys 2004, 42, 3775.
31. Vyazovkin, S. Macromol Rapid Commun 2002, 23, 771.
32. Vyazovkin, S.; Sbirrazzuoli, N. J Therm Anal 2003, 72, 681.
33. Turnbull, D.; Fisher, J. C. J Chem Phys 1949, 17, 71.